Detection of surface algal blooms using the newly developed algorithm surface algal bloom index (SABI)

Fahad Alawadi*[a]

[a]School of Ocean and Earth Science, University of Southampton,
Waterfront Campus, Empress Dock, Southampton, S014 3ZH, UK

ABSTRACT

Quantifying ocean colour properties has evolved over the past two decades from being able to merely detect their biological activity to the ability to estimate chlorophyll concentration using optical satellite sensors like MODIS and MERIS. The production of chlorophyll spatial distribution maps is a good indicator of plankton biomass (primary production) and is useful for the tracing of oceanographic currents, jets and blooms, including harmful algal blooms (HABs). Depending on the type of HABs involved and the environmental conditions, if their concentration rises above a critical threshold, it can impact the flora and fauna of the aquatic habitat through the introduction of the so called "red tide" phenomenon. The estimation of chlorophyll concentration is derived from quantifying the spectral relationship between the blue and the green bands reflected from the water column. This spectral relationship is employed in the standard ocean colour chlorophyll-a (Chlor-a) product, but is incapable of detecting certain macro-algal species that float near to or at the water surface in the form of dense filaments or mats. The ability to accurately identify algal formations that sometimes appear as oil spill look-alikes in satellite imagery, contributes towards the reduction of false-positive incidents arising from oil spill monitoring operations. Such algal formations that occur in relatively high concentrations may experience, as in land vegetation, what is known as the "red-edge" effect. This phenomena occurs at the highest reflectance slope between the maximum absorption in the red due to the surrounding ocean water and the maximum reflectance in the infra-red due to the photosynthetic pigments present in the surface algae. A new algorithm termed the surface algal bloom index (SABI), has been proposed to delineate the spatial distributions of floating micro-algal species like for example cyanobacteria or exposed inter-tidal vegetation like seagrass. This algorithm was specifically modelled to adapt to the marine habitat through its inclusion of ocean-colour sensitive bands in a four-band ratio-based relationship. The algorithm has demonstrated high stability against various environmental conditions like aerosol and sun glint.

Keyword List: surface algal bloom index, SABI, algae, MODIS, ROPME, HABs, NDVI, oil spill.

1. INTRODUCTION

Oceanographers have studied satellite data in order to measure ocean color, from which they have been able to derive chlorophyll a (Chlor-a) concentration and phytoplankton biomass in open oceans (case I waters). This process started with the Coastal Zone Color Scanner (CZCS)[1,2]; and continued with a number of sensors: Ocean Color and Temperature Scanner–OCTS[3]; Sea-viewing Wide Field-of-view Sensor–SeaWiFS[4]; the Moderate Resolution Imaging Spectroradiometer–MODIS[5]; and the Medium Resolution Imaging Spectrometer – MERIS[6]. Chlorophyll causes a shift in the blue to green ratio of upwelling light in case I waters, where the optical properties mainly depend on phytoplankton[7,8]. The MODIS 500 m resolution Chlor-a algorithm was generated according to Equation (1):

$$\log(\mathrm{Chlor_a}) = 0.1464 - 1.7953R + 0.9718R^2 - 0.8319R^3 - 0.8073R^4 \quad (1)$$

where R is defined as:

* fa2x07@soton.ac.uk; fahad@ropme.org

Remote Sensing of the Ocean, Sea Ice, and Large Water Regions 2010, edited by Charles R. Bostater Jr., Stelios P. Mertikas, Xavier Neyt, Miguel Velez-Reyes, Proc. of SPIE Vol. 7825, 782506 · © 2010 SPIE
CCC code: 0277-786X/10/$18 · doi: 10.1117/12.862096

$$10^{R} = \frac{\rho_{rs}(469)}{\rho_{rs}(555)} \tag{2}$$

where ρ_{rs} is the remote sensing reflectance at the corresponding blue (B_3=469 nm) and green (B_4=555 nm) bands respectively. Equation (2) has to yield a positive value to produce a valid Chlor-a pixel value, otherwise Chlor-a would fail to be evaluated for that particular pixel. This failure can be caused by the presence of absorbing aerosols that cannot be detected by the atmospheric correction process[9], causing an overestimation of the atmospheric contribution in all bands. This overestimation will induce severe errors, particularly at the shorter wavelengths, that might even cause total failure in the production of Chlor-a[10]. Another reason for the failure of Chlor-a is infra-red (IR) reflectance caused by the presence of large concentrations of Chlor-a at the water surface or very close to it, which is a direct violation of the dark pixel assumption over clear water.

Algae is a non-planktonic species that performs photosynthesis. It is commonly classified into two groups: macro-algae like seaweed and micro-algae like filamentous cyanobacteria. They are also divided into three groups based on their photosynthetic pigments: Phaeophyta (the browns), Rhodophyta (the reds) and Chlorophyta (the greens), but can also appear in various other colour combinations like yellow or silvery grey. They are capable of regulating their buoyancy to modulate their photosynthetic activity to the changing light levels. This mechanism of buoyancy is either to protect themselves from excessive radiation[11] or to access more light from the photic region located in the top layer of the water surface[11,12]. Surface emerging algae can experience, similar to land-based vegetation, the "red-edge" effect, where the greatest reflectance slope occurs between the maximum absorption in the red and the maximum reflection in the infra-red (0.7 μm-1.0 μm). The IR reflectance is caused by the combination of decreasing absorption by the chlorophyll pigments in the spongy mesophyll cells and the increasing of absorption by water[13-15]. Texturally, surface blooms are often characterized by their thick extensive mats or scum that looks like oil slicks or slightly foamy pollution.

Equation (3) shows the normalized difference vegetation index (NDVI) that was proposed by Rouse et al. (1974)[16] to measure the vegetation activity at the land surface. It normalizes the output from –1 to +1, to partially account for the differences in illumination and surface slope. Researchers like Kahru et a1 (1993)[17] have examined the use of NDVI on surface cyanobacterial blooms, but more recent algorithms were proposed specifically for the detection of surface algae like for example the Maximum Chlorophyll Index (MCI); the Spectral Contrast Shift (SCS); and the MODIS Floating Algae Index (FAI) proposed by Gower et al. (2005)[18], Alawadi et al. (2008)[19] and Hu (2009)[20] respectively.

$$\mathrm{NDVI} = \frac{X_{NIR} - X_R}{X_{NIR} + X_R} \tag{3}$$

where X can be the top-of-atmosphere (TOA) radiance (L_t) – provided that it was measured in the same irradiance conditions for both bands; TOA reflectance (ρ) or ρ_{rs} at the near-infrared (NIR) and the red (R) bands. In the case of MODIS, the 250 m resolution bands are used at B_1 (R =645 nm) and B_2 (NIR=869 nm).

1.1 The Surface Algal Bloom Index (SABI)

The SABI is an empirical algorithm developed in order to detect water floating biomass that has a NIR response similar to that of land vegetation, with the specific inclusion of ocean-sensitive spectral bands; the blue (characteristic of clear water) and green (characteristic of the water column bloom):

$$\mathrm{SABI} = \frac{X_{NIR} - X_R}{X_B + X_G} \tag{4}$$

where X has been defined earlier for Equation (3), at the following MODIS wavelengths: B_1 (X_R=645 nm) and B_2 (X_{NIR}=869 nm), both aggregated from the 250 m resolution MODIS band group; and bands B_3 (X_B=469 nm) and B_4 (X_G=555 nm), respectively available within the 500 m resolution MODIS band group.
The SABI formula is a ratio dependent relation, making it advantageous in cancelling out a large proportion of signal variations arising from the variations in the intensity of incident light that accompany different sun angles,

clouds/shadow and atmospheric conditions[21]. It will however, not account for the spectral dependencies generated by the additive atmospheric (path radiance) effects. The inclusion of the blue and green bands in the denominator, and the subtraction of the red band in the numerator (Equation 4), are collectively expected to make the SABI less sensitive to atmospheric effects, particularly for those that are sensitive to the red and green bands. It is also expected to reduce the effect of molecular scattering (Rayleigh scattering) particularly at shorter wavelengths.

2. METHOD

For this analysis, the relation for the TOA reflectance (ρ) that was used:

$$\rho(\lambda)=\frac{\pi L_t(\lambda)}{F_0(\lambda)\cos\theta} \tag{5}$$

where L_t is the calibrated TOA radiance; F_0 is the extraterrestrial mean solar irradiance, and θ is the solar zenith angle – the angle between the line from the pixel under examination to the sun and the local vertical.

When substituting Equation (5) into Equation (4), the accuracy of the SABI will only depend on the uncertainties that exit in L_t and F_0.

Although it is the ρ_{rs} – produced after performing atmospheric correction, that is required as input in algorithms for deriving most of the MODIS ocean products[22,23], the ρ was used instead. This is because performing atmospheric correction was deemed unnecessary at this preliminary phase, since the aim was to map the extent of algal blooms instead of producing a biophysical parameter like concentration[24,25]. Furthermore, the atmospheric correction assumes that case I type waters to have zero water-leaving radiance at the NIR bands (B_2=869 nm and B_{15}=748 nm for MODIS), which conflicts with the red-edge effect exhibited by surface algae.

The SeaWiFS Data Analysis System (SeaDAS) version 6.0 was used to process MODIS L1B TOA calibrated radiances to produce the ρ and other bio-optical products for correlation purposes like for example Chlor-a, Sea Surface Temperature (SST) and the Aerosol optical thickness at 869 nm (tau_869). Non-geometrically corrected images were also produced representing the natural RGB colour composite, corresponding to bands 1,4,3 (B_1=645 nm, B_4=555 nm, B_3=469 nm) in the 500 m/pixel resolution, and a false RGB colour composite corresponding to the aggregated bands 2,1,1 in the 500 m/pixel resolution bands (B_1=645 nm, B_2=869 nm). The reason for composing these images was to identify the natural colour of the bloom as it appears in the case of 143, and in the case of the 211 colour composite, to highlight the near-surface algae by appearing reddish in colour due to the NIR reflectance. The standard masks produced by SeaDAS during the atmospheric correction process like for example the cloud and sun glint masks were also used to test their masking quality over the valid surface algae pixels.

3. RESULTS

Figure 1 shows the location map of the different datasets on which SABI was tested and the TOA spectral characteristics plot for the species involved, with respect to MODIS 500 m bands.

3.1 Sargassum– Gulf of Mexico

Sargassum is characterized by having elongated, narrow fronds and numerous spherical gas-filled bladders called vesicles allowing the plant to float freely[26]. The colour of Sargassum can vary from yellow to brown to black[27].

Figure 2 shows a sample taken from swath number (1) representing partly exposed sargassum patches with most of them submerged below the water surface, as they appear in the products of the Chlor-a, SABI, 143 and 211 colour composites taken from Terra on 02 June 2006.

The mean wind speed derived from QuikScat at the sample area was 4±2 ms^{-1}. Table 1 shows the SABI, NDVI and Chlor-a values at selected points appearing in Figure 2. The SST for the bloom (not shown) did not reveal significant

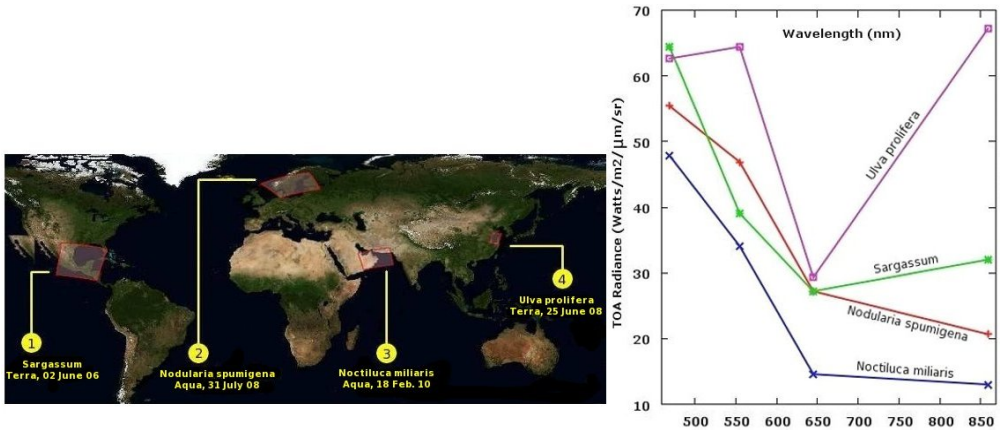

Figure 1. The location map of the different MODIS swaths where the SABI was tested on (left), and the TOA spectral characteristics of the surface floating species detected in relation to MODIS 500 m bands (right).

temperature variability with the surrounding waters except at point C (SABI > 0), where it was flagged with poor quality. This is caused because the 3x3 pixel neighbourhood to point C were: (1) experiencing saturation or non spatial uniformity in the red band (B_{14}=678 nm) reflectance; and (2) the SST retrieval was cold relative to the reference[28]. At point B, the SABI was negative, indicating a water column bloom; which was confirmed by the presence of a valid Chlor-a value. Clouds were distinguishable from the colour and shape that they appeared within the 143 and 211 images, although a small percentage of them were misclassified as surface algae in the SABI relation.

Table 1: The SABI, NDVI and Chlor-a values at points A, B and C respectively shown in Figure 2.

Point Description	SABI	NDVI	Chlor-a (mg m^{-3})
A (thin clouds)	– 0.03	– 0.04	Non valid data
B (water column sargasum)	– 0.04	– 0.1	0.03
C (surface sargasum)	0.1	0.2	Non valid data

3.2 *Nodularia spumigena*– Baltic Sea

Nodularia spumigena is a hepatotoxic cyanobacterium[29] that can colour the water green, blue-green or yellow. Figure 3 shows a sample taken from swath number (2) of the *N. spumigena* bloom as it appears in the images of 211, 143, SST, SABI and Chlor-a images, taken from MODIS Aqua on 31 July 2008. The figure also shows a spectral plot of at the 500 m bands, selected points appearing in the 143 colour composite. The mean wind speed derived from QuikScat at the sample area was 5±2 ms^{-1}.

According to Figure 3, the bloom's temperature at point A was found to be 3% higher than its surrounding waters, which agrees with the findings of Kahru et al. (1993)[17] and Sato et al. (1998)[30], that the presence of SST 'hot spots' is an indicator of near-surface phytoplankton.

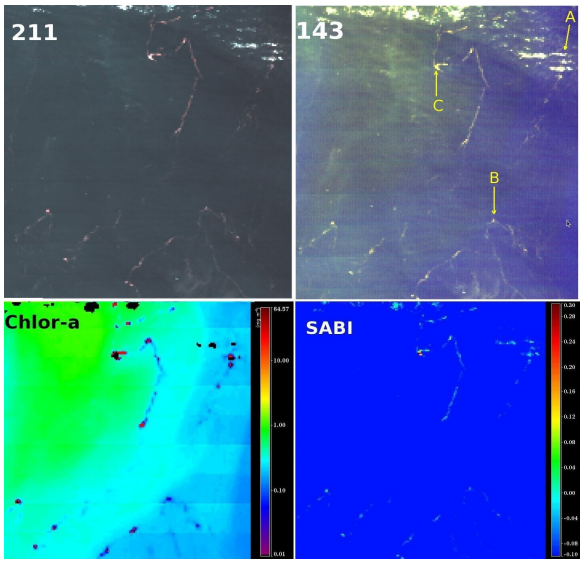

Figure 2. Sargassum in the Gulf of Mexico (Terra, 02 June 2006) representing partly exposed patches and mostly submerged below the water surface as they appear in the products of the 211 and 143, Chlor-a and the SABI images in the 500 m resolution. In the Chlor-a image, point C was misclassified as cloud, and the failed Chlor-a pixels were masked in red.

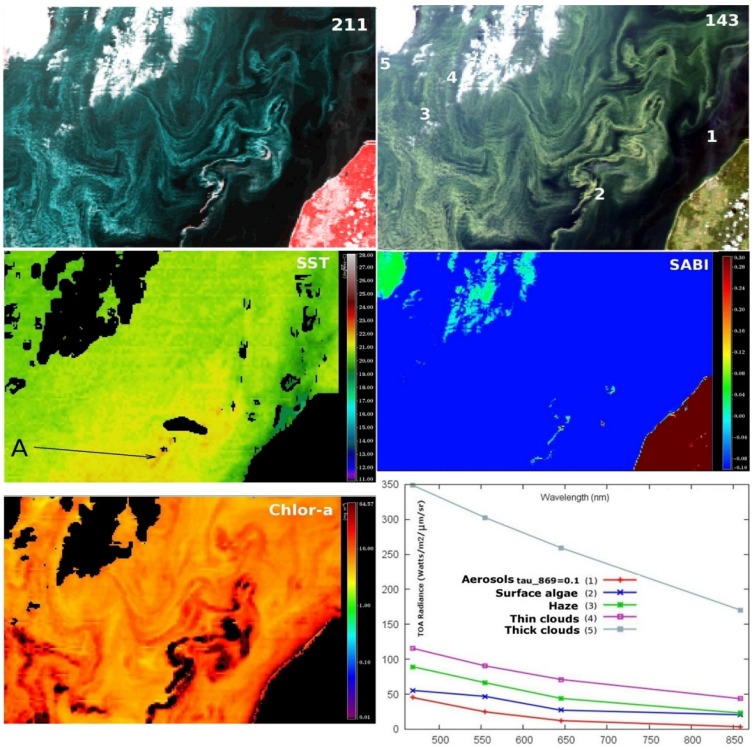

Figure 3. *N. spumigena* bloom in the Baltic Sea (Aqua, 31 July 2008) as it appears in the images of 211, 143, SST, SABI and Chlor-a . The SST at point A is 3% higher than surrounding water temperature. A spectral plot at the 500 m bands is shown for selected points appearing in the 143 colour composite.

3.3 *Noctiluca miliaris*– Arabian Sea

Noctiluca miliaris (synonym *Noctiluca scintillans* Macartney*)* is a large cosmopolitan marine dinoflagellate[31]. A number of studies have tried to explain the negative relationship that exists between non-photosynthetic species like *N. miliaris.a* and other phytoplanktonic species by indicating the need for *Noctiluca* to have relatively high quantity of its phytoplankton prey to support its optimal growth[32,33], during which the diatom bloom *N. scintillans* increases, as the algal biomass decreases[34].

Figure 4 shows a bloom of such species that appear in the SABI, SST, Chlor-a, 143 and the NDVI images, taken from MODIS Aqua on 18 Feb 2010. Figure 4 also shows two line transect profiles across varying aerosol layer and a sun glint region. From this plot, both the NDVI and the SABI have decreased by 15% and 3%, as the aerosol layer changed its density from low (tau_869=0.07) to high (tau_869=0.17) respectively. The sun glint transect plot shows that the SABI was less sensitive to the effect of sun glint than the NDVI.

Only 2% of the failed Chlor-a pixels had a positive SABI values (floating at water surface), leaving the bulk of failed pixels having negative SABI values, that is submerged under water but close to its surface. The positive SABI pixel values were also flagged out in the SST product for the same reasons that were described earlier for the Baltic Sea area.

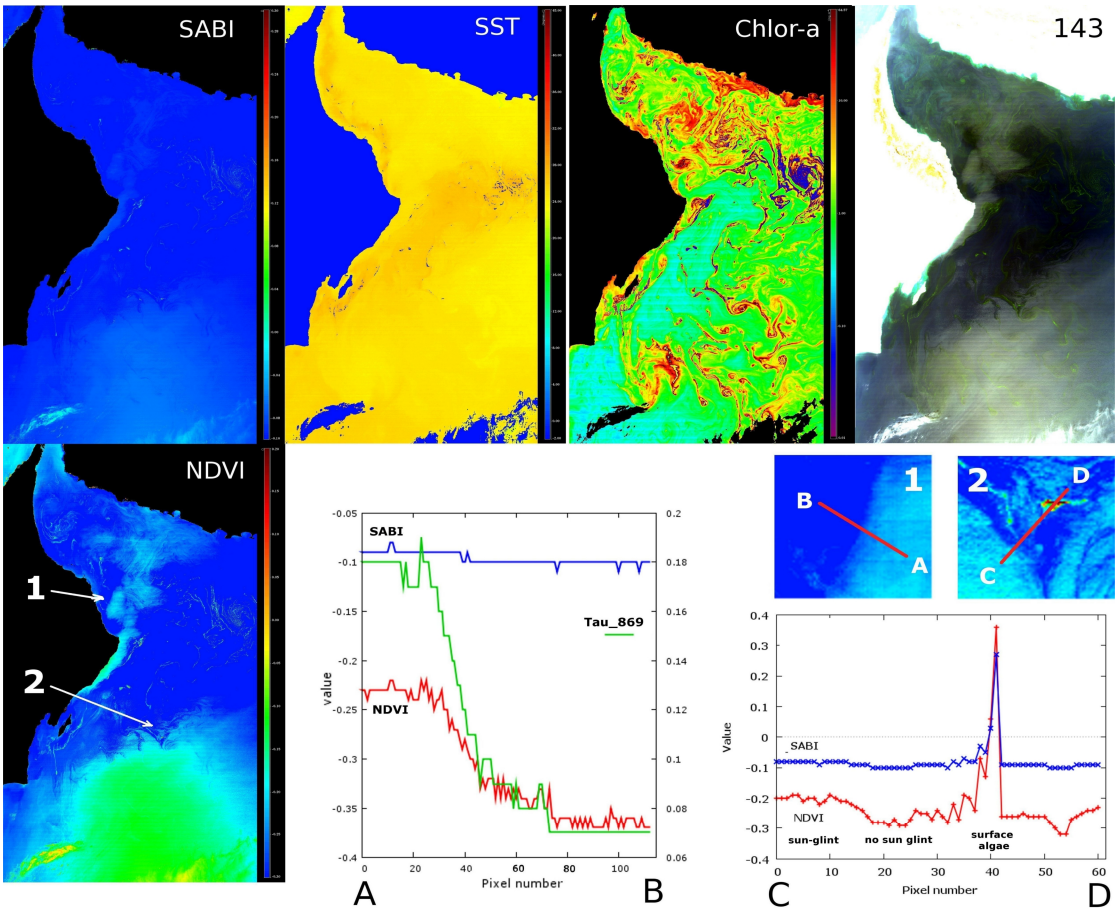

Figure 4. *N. miliaris* bloom in the Arabian Sea (Aqua, 18 Feb 2010) as it appears in the, SABI, SST, Chlor-a, NDVI and 143 colour images. Two line-transect plots across varying aerosol layer (region 1) and sun glint (region 2) from (A to B) and (C to D) respectively. The failed Chlor-a and SST pixels are masked in blue and black respectively.

3.4 *Ulva prolifera* – Yellow Sea

Ulva prolifera is unattached filamentous green macroalgae formerly known as *Enteromorpha prolifera*[35]. Figure 5 shows a bloom for the *Ulva prolifera* species directly under the sun glint as they appear in the SST, 211, NDVI and the SABI images on the coastline of Qingdao, in eastern China taken from MODIS Terra on 25 June 2008. Although the wind speed data was not available from QuikScat during that time, it is possible to estimate it to be not more than ~ 8 ms^{-1}, since an increase in wind velocity above 6–8 ms^{-1} results in the dispersion of such aggregates[17,36]. The Chlor-a product could not be retrieved mainly due to sun glint, which changed the reflectance magnitude rather than the spectral shape[37,38]; and probably due to the high turbidity caused by the suspended sediments, which affect the distribution of planktonic and benthic organisms in the coastal waters of the Yellow Sea[39,40].

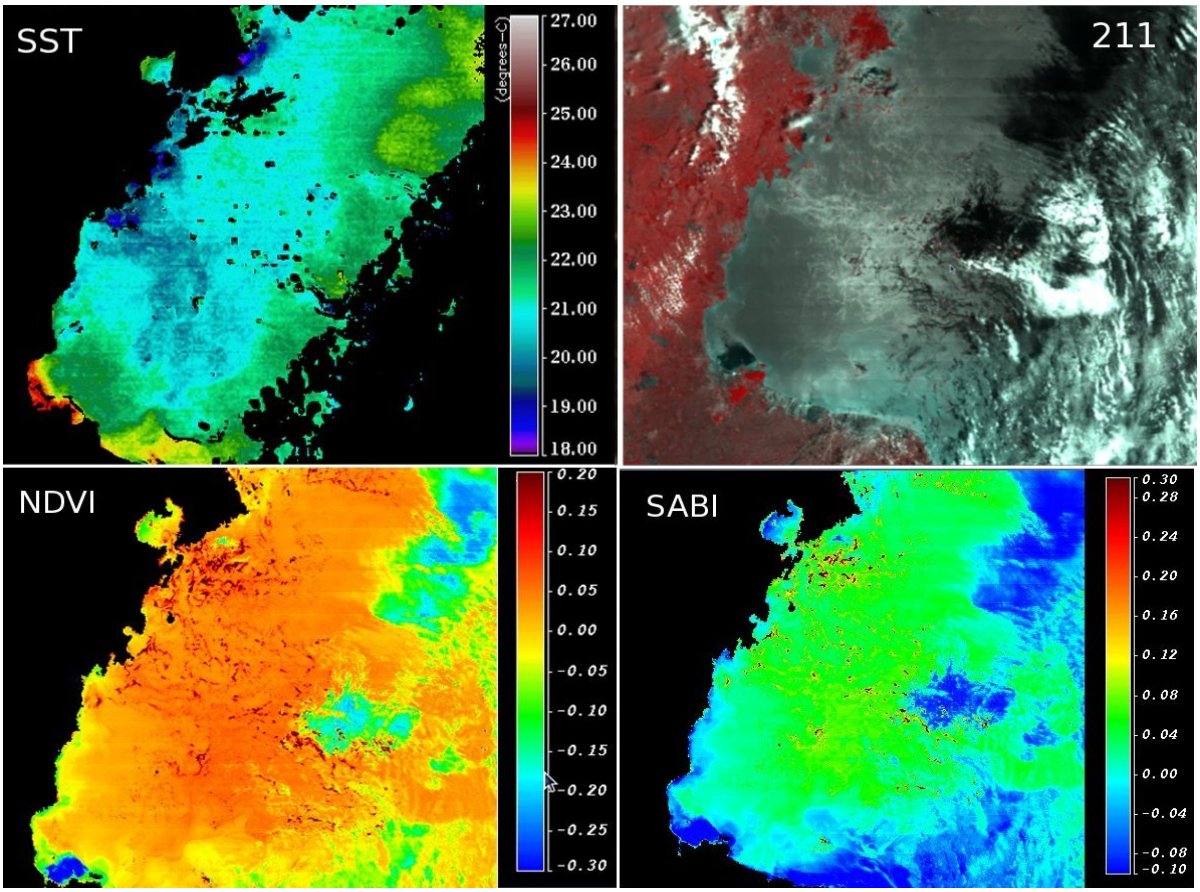

Figure 5. *Ulva prolifera* bloom in the Yellow Sea (Terra, 25 June 2008) directly under the sun glint as it appears in the SST, 211, NDVI and SABI images.

3.5 Oil spill response in the SABI and NDVI

Figure 6 shows an oil spill located at (59°14' 39" N, 22°10' 29" E) in the Baltic Sea dataset, with a line transect plot across the oil spill and water (clear and turbid) shown in the NDVI and the SAB. The figure also shows a spectral plot of the corresponding oil and water at the 500 m bands. The SABI has demonstrated less sensitivity to the presence of oil and turbid water than did the NDVI. This is because spectrally a thin layer of oil (sheen) is very similar to water (optically transparent). However, this sensitivity will vary depending on the type of oil (refractive index) and texture (weathering condition).

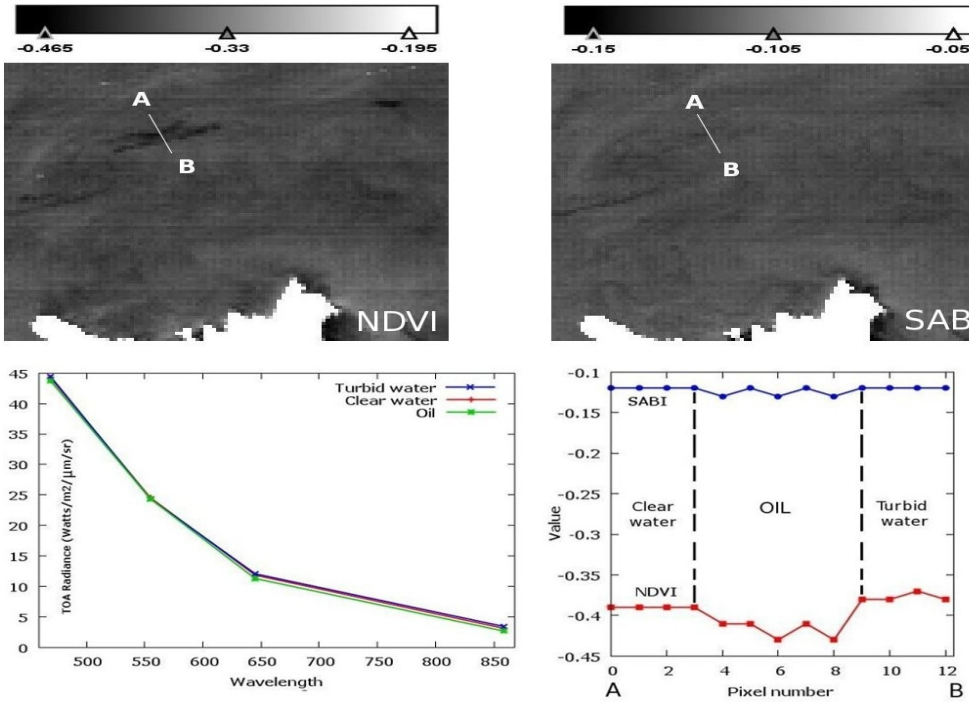

Figure 6. An oil spill located at (59°14' 39" N, 22°10' 29" E) taken from the Baltic Sea dataset. The line transect plots across an oil spill and water (clear and turbid) from (A to B) shown for the SABI and NDVI images created from TOA radiances, together with a spectral plot of the corresponding oil and water.

Figure 7 shows the Gulf of Mexico oil spill taken from MODIS Aqua on 25 April 2010, where a line transect plot is shown for both the NDVI and the SABI images. In both cases, the SABI value for oil was smaller than that for surface algae. It is possible however, to discriminate between oil spills and surface algae using non-spectral methods, like for example the oil spread index (OSI) that was developed by Alawadi (2009)[41]. Such methods mainly rely on discriminating between oil spills and their look-alikes, like surface algae, based on the distinct texture and shape features that each make at the water surface.

3.6 Statistical analysis

Figure 8 shows the SABI (sample number N=606) and NDVI (N=824) box plots for a two-class sample containing water (with or without water column bloom) and surface floating algae taken from each of the sea area datasets. The mean SABI values, appear to have higher stability in relation to the different atmospheric conditions and types of species. As in the case of the Yellow Sea, its extreme mean reflectance value could be attributed to: (1) the presence of the bloom directly under the sun glint; (2) the high Chlor-a concentration that existed in the floating *Ulva prolifera* species at the time; and (3) the high turbidity in the East China Sea which is a typical case II water environment, where the concentrations of phytoplankton pigments, suspended matter, and chromophoric dissolved organic matter (CDOM) are all higher than those in the open oceans[42]. In all of the examples, the difference between the maximum SABI values to the mean was larger than the difference from its minimum due to the abundance of the water class in the samples. The standard error estimated from the collective means of all datasets was 0.14 and 0.24 for the SABI and NDVI respectively, which again further indicates the stability of the SABI algorithm.

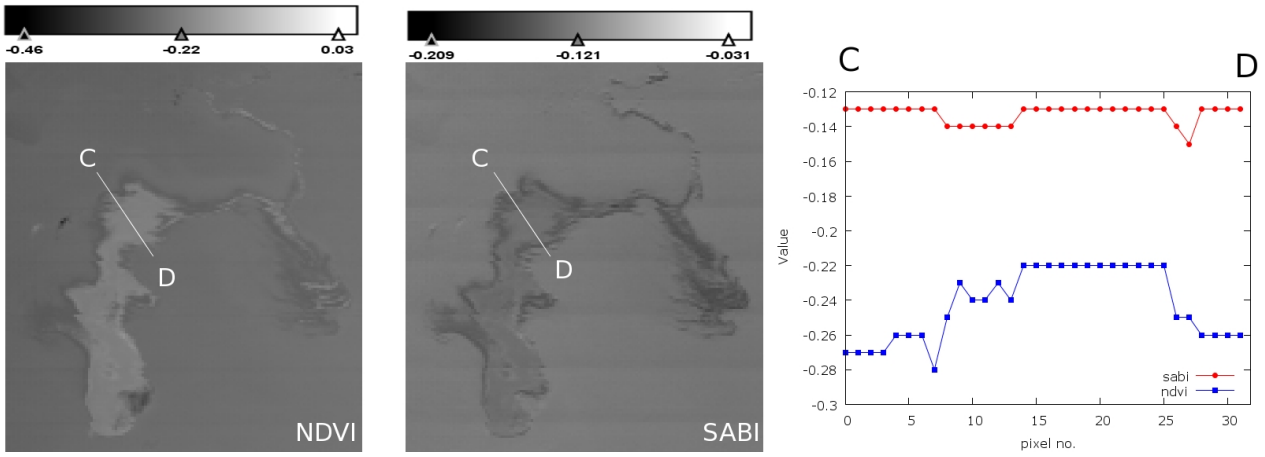

Figure 7. An image of the Gulf of Mexico oil spill (Aqua, 25 April 2010). A line transect plot across the spill from points C to D, is shown for the NDVI and the SABI images created from TOA radiances.

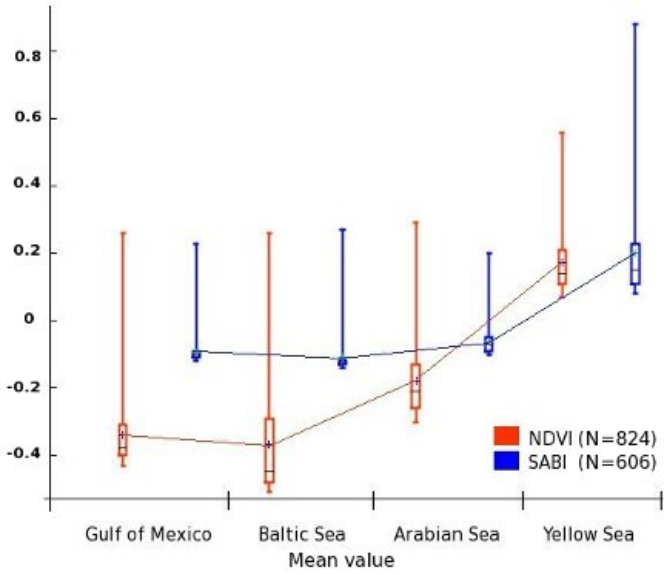

Figure 8. Box plots of the mean NDVI and SABI values for each of the datasets. The samples contain two classes: water (with and without bloom) and surface floating algae.

3.7 SABI AND NDVI in TOA radiance (L_t)

Figure 9 shows how the SABI has demonstrated better delineation results for surface floating algae than the NDVI when using TOA radiance (L_t) instead of reflectance. This is probably because 90% of the scattering originates from the atmosphere particularly in the shorter visible wavelengths, and therefore, according to Equation (4), the overall SABI value will be much smaller than in the NDVI.

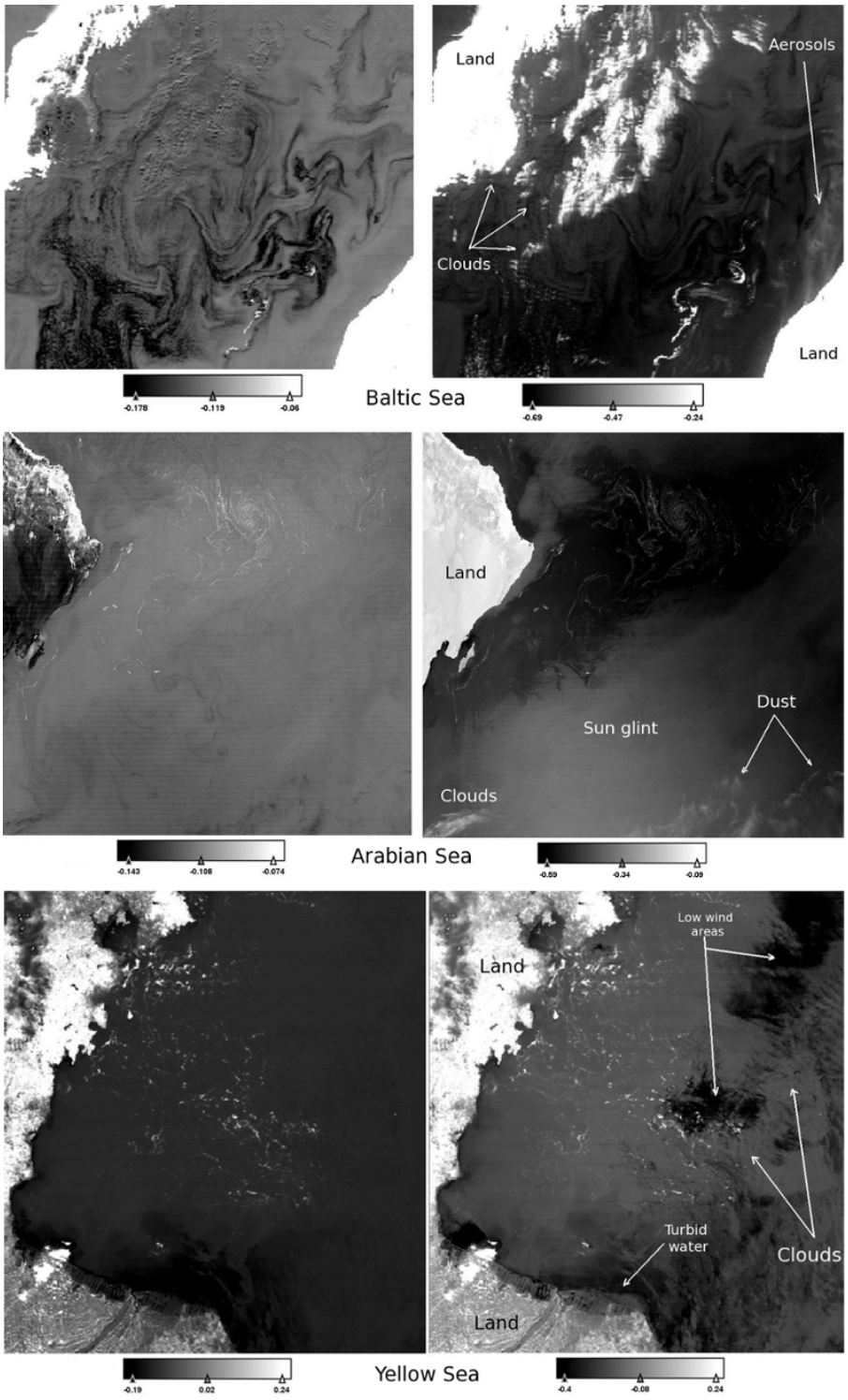

Figure 9. The SABI (left) and NDVI (right) created from TOA radiance for the Baltic, Arabian and Yellow seas.

4. CONCLUSION

The surface algal bloom index (SABI) is a four-band algorithm developed to map the spatial distribution of surface and near-surface algae in global oceans. It achieves this by using the red-edge effect as a tool to distinguish floating algae in a background of clear blue water and/or green planktonic water-mixed blooms. SABI's robustness is attributed to the following factors: (1) it is a ratio-based relationship applicable to spectral radiances (if measured at the same irradiance conditions) and reflectances, making it relatively insensitive to many of the uncertainties introduced by the bidirectional reflectance distribution function (BRDF); (2) it is a four-band relationship, that will distribute the weight of each optical response proportionally; and (3) the inclusion of short wave bands (green and blue) in the denominator of the ratio making it: (a) highly suitable for relating near-surface bloom distributions to those occurring at the water surface; and (b) highly stable against sun glint as well as a number of optical scattering sources in the atmosphere, like molecules and certain particles.

The SABI formulae used MODIS wavebands that belong to the 500 m spatial resolution group: B_1 (R=645 nm) and B_2 (NIR=869 nm) both aggregated from the 250 m resolution MODIS band group; and bands B_3 (B=469 nm) and B_4 (G=555 nm).

Positive SABI values are a relative measure of the photosynthetic activity exhibited by the surface algae. Whereas negative values will point to the species' state of buoyancy in the water relative to their photosynthetic activity. This would, therefore, indicate either that the species are found deeper in the water column, leading to high water absorption in the NIR and preventing the red-edge effect from being detected, or the species are simply no longer photosynthetically active.

Case II and the highly productive case I waters may have significant contributions in the NIR, incompatible with the dark pixel assumption used in the standard atmospheric correction operation. This can lead to significant under-estimation of the derived water-leaving radiances. Similarly, MODIS standard cloud and sun glint masks were found to mask valid pixels containing surface algae. For this reason, the apparent reflectance were used instead of the surface water reflectance.

The detection of surface-floating algae was possible in moderate wind speeds that do not exceed average speeds greater than ~ 8 ms^{-1}, otherwise such formations will be dispersed by the sea waves.

MODIS bio-physical products like Chlor-a and SST are useful data in providing complementary information on surface algae. For example, positive SABI values was one of the reasons for the failure of Chlor-a, though not exclusively.

Surface blooms did exhibit an average temperature increase of 2 °C compared to the surrounding water temperature. This was probably caused the presence of surface algae that absorbs more of the solar energy in the immediate surface layer.

For the detection of surface algae, both the NDVI and the SABI share the same red-edge term in their numerators. However, because the SABI has included the highly sensitive ocean-colour bands in its denominator, it has shown superior stability against the various interfering conditions like sun glint, aerosols and turbid case II waters.

According to the SABI scale, oil will always have smaller SABI values than surface or near-surface algal blooms (i.e. < -0.1) regardless of the type of oil involved in the spill. Such characteristic qualifies the SABI algorithm to be a good discriminator of oil from such look-alike species. Thermally, oil did not demonstrate any significant temperature variability to its surrounding water as algae did.

Finally, further research remains open to address issues like: the applicability of the SABI algorithm with other corresponding wave bands implemented by different optical sensors like MERIS; and the validation process of the algorithm via *in situ* measurements.

ACKNOWLEDGEMENTS

Special thanks are due to Dr. Peter Petrov; Dr. Valborg Byfield; and Prof. Carl Amos for their valuable contribution towards the preparation of this paper.

5. REFERENCES

[1] Gordon, H.R., Clark, D.K., Brown, J.W., Brown, O.B., Evans, R.H., and Broenkow, W.W., "Phytoplankton pigment concentrations in the Middle Atlantic Bight: comparison of ship determinations and CZCS estimates," Appl. Opt 22, 20–36 (1983).

[2] Hovis, W.A., Clark, D.K., Anderson, F., Austin, R.W., Wilson, W.H., Baker, E.T., Ball, D., Gordon, H.R., Mueller, J.L., et al., "Nimbus-7 Coastal Zone Color Scanner: System Description and Initial Imagery," Science 210(4465), 60-63 (1980).

[3] Iwasaki, N., Kajii, M., Tange, Y., Miyachi, Y., Tanaka, T., Sato, R., and Inoue, K., "Status of ADEOS mission sensors," Acta Astronautica 28, 139-146 (1992).

[4] Hooker, S.B., Esaias, W.E., Feldman, G.C., Gregg, W.W., and McClain, C.R., "An Overview of SeaWiFS and Ocean Color, Vol. 1 of SeaWiFS Technical Report Series," NASA tech. memo 104566, (1992).

[5] Salomonson, V.V., Barnes, W.L., Maymon, P.W., Montgomery, H.E., and Ostrow, H., "MODIS: advanced facility instrument for studies of the Earth as asystem," IEEE Transactions on Geoscience and Remote Sensing 27(2), 145–153 (1989).

[6] Rast M., and Bezy J. L., "The ESA Medium Resolution Imaging Spectrometer MERIS a review of the instrument and its mission," International Journal of Remote Sensing 20, 1681-1702 (1999).

[7] Morel, A., and Prieur, L., "Analysis of Variations in Ocean Color," Limnology and Oceanography 22(4), 709-722 (1977).

[8] Prieur, L., and Sathyendranath, S., "An optical classification of coastal and oceanic waters based on the specific spectral absorption curves of phytoplankton pigments, dissolved organic matter, and other particulate materials," Limnology and Oceanography 26(4), 671–689 (1981).

[9] Werdell, P.J., Franz, B.A., Bailey, S.W., Harding Jr, L.W., and Feldman, G.C., "Approach for the long-term spatial and temporal evaluation of ocean color satellite data products in a coastal environment," in Proc. of SPIE Vol 6680, 66800G–1 (2007).

[10] Wang, M., "The SeaWiFS atmospheric correction algorithm updates," SeaWiFS postlaunch calibration and validation analyses, Part 1, 2000–206892 (2000).

[11] Franklin, L.A., and Forster, R.M., "The changing irradiance environment: consequences for marine macrophyte physiology, productivity and ecology," European Journal of Phycology 32(3), 207 (1997).

[12] Paerl, H.W., and Ustach, J.F., "Blue-green algal scums: an explanation for their occurrence during freshwater blooms," Limnology and oceanography 27(2), 212–217 (1982).

[13] Sellner, K.G., "Physiology, ecology, and toxic properties of marine cyanobacteria blooms," Limnology and Oceanography 42(5), 1089–1104 (1997).

[14] Tucker, C.J., "Red and photographic infrared linear combinations for monitoring vegetation," Remote Sensing of Environment 8(2), 127-150 (1979).

[15] Jackson, R., Slater, P., and Pinter Jr., P., "Discrimination of growth and water stress in wheat by various vegetation indices through clear and turbid atmospheres," Remote Sensing of Environment 13(3), 187-208 (1983).

[16] Rouse, J.W., Haas, R.H., Schell, J.A., Deering, D.W., and Harlan, J.C., "Monitoring the vernal advancement and retrogradation (green wave effect) of natural vegetation," NASA/GSFC Type III Final Report, Greenbelt, Md 371, (1974).

[17] Kahru, M., Leppänen, J.M., and Rud, O., "Cyanobacterial blooms cause heating of the sea surface," Marine Ecology-Progress Series 101, 1–1 (1993).
[18] Gower, J., King, S., Borstad, G., and Brown, L., "Detection of intense plankton blooms using the 709 nm band of the MERIS - imaging spectrometer," International Journal of Remote Sensing 26(9), 2005 (2005).
[19] Alawadi, F., Amos, C., Byfield, V., and Petrov, P., "The application of hyperspectral image techniques on MODIS data for the detection of oil spills in the RSA," in Proceedings of SPIE, 71100Q-71100Q-12 (2008).
[20] Hu, C., "A novel ocean color index to detect floating algae in the global oceans," Remote Sensing of Environment 113(10), 2118-2129 (2009).
[21] Huete, A.R., Justice, C.O., and Van Leeuwen, W.J.D., [MODIS Vegetation Index (MOD 13). Version 3. Algorithm Theoretical Basis Document] , Technical report, http://modis. gsfc. nasa. gov/data/atbd/land atbd. html (1999).
[22] Lee, Z., Carder, K.L., Steward, R.G., Peacock, T.G., Davis, C.O., and Mueller, J.L., "Remote sensing reflectance and inherent optical properties of oceanic waters derived from above-water measurements," in Ocean Optics XIII 2963, S. G. Ackleson and R. J. Frouin, Eds., 160-166 (1997).
[23] Mueller, J.L., Zaneveld, J.R., Pegau, S., Valdez, E., Maske, H., Alvararez-Borrego, S., and Lara-Lara, R., "Remote sensing reflectance: preliminary comparisons between in-water and above-water measurements, and estimates modeled from measured inherent optical properties," Ocean Optics XIII502–507 (1997).
[24] Robinson, I.S., [Measuring the oceans from space: the principles and methods of satellite oceanography] , Springer Verlag (2004).
[25] Metsamaa, L., Kutser, T., and Stroembeck, N., "Recognising cyanobacterial blooms based on their optical signature: a modelling study," Boreal Environment Research 11(6), 493–506 (2006).
[26] Littler, D.S., Littler, M.M., Bucher, K.E., and Norris, J.N., [Marine plants of the Caribbean] , Smithsonian Institution Press (1989).
[27] Hacker, S.D., and Madin, L.P., "Why habitat architecture and color are important to shrimps living in pelagic Sargassum: Use of camouflage and plant-part mimicry.," Marine ecology progress series. Oldendorf 70(2), 143–155 (1991).
[28] Franz, B.A., "Implementation of SST Processing within the OBPG," http://oceancolor.gsfc.nasa.gov/DOCS/modis_sst/, 2006 (4 April 2010).
[29] Kononen, K., "Dynamics of the toxic cyanobacterial blooms in the Baltic Sea," Finnish Institute of Marine Research, Helsinki (1992).
[30] Sato, M.S., Suzuki, M., and Hayashi, H., "The Density of a Homogeneous Population of Cells Controls Resetting of the Program for Swarmer Formation in the Unicellular Marine MicroorganismNoctiluca scintillans," Experimental Cell Research 245(2), 290-293 (1998).
[31] Bhimachar, B., and George, P., "Abrupt set-backs in the fisheries of the malabar and kanara coasts and "red water" phenomenon as their probable cause," Proceedings: Plant Sciences 31(6), 339-350 (1950).
[32] Lee, J.K., and Hirayama, K., "Effects of salinity, food level and temperature on the population growth of Noctiluca scintillans (Macartney)," Bulletin of the Faculty of Fisheries-Nagasaki

University (Japan) (1992).
[33] Kioeboe, T., and Titelman, J., "Feeding, prey selection and prey encounter mechanisms in the heterotrophic dinoflagellate Noctiluca scintillans," Journal of Plankton Research 20(8), 1615–1636 (1998).
[34] Nakamura, Y., "Biomass, feeding and production of Noctiluca scintillans in the Seto Inland Sea, Japan," Journal of Plankton Research 20(11), 2213 (1998).
[35] Hayden, H., Blomster, J., Maggs, C., Silva, P., Stanhope, M., and Waaland, R., "Linnaeus was right all along: Ulva and Enteromorpha are not distinct genera," European Journal of Phycology 38(3), 277-294 (2003).
[36] Mazur-Marzec, H., and Plinski, M., "Do toxic cyanobacteria blooms pose a threat to the Baltic ecosystem?," Oceanologia 51(3), 293–319 (2009).
[37] Gons, H.J., "Optical Teledetection of Chlorophyll a in Turbid Inland Waters," Environmental Science & Technology 33(7), 1127-1132 (1999).
[38] Gons, H.J., Rijkeboer, M., Bagheri, S., and Ruddick, K.G., "Optical Teledetection of Chlorophyll a in Estuarine and Coastal Waters†," Environmental Science & Technology 34(24), 5189-5192 (2000).
[39] Tang, Q., "Changes in the biomass of the Yellow Sea ecosystem," in Biomass Yields and Geography of Large Marine Ecosystems. Shernmn K and LM Alexander (eds.). AAAS Selected Symposium. Westvie'a Press Inc, Boulder, CO, USA, 7–35 (1989).
[40] Zhang, C.I., and Kim, S., "Living marine resources of the Yellow Sea ecosystem in Korean waters: status and perspectives," Large Marine Ecosystems of the Pacific Rim: Assessment, Sustainability, and Management.. Sherman, K. and Q. Tang. Blackwell Science. Malden, MA163–178 (1999).
[41] Alawadi, F., "New pattern recognition methods for identifying oil spills from satellite remote sensing data," in Society of Photo-Optical Instrumentation Engineers (SPIE) Conference Series 7477, 29 (2009).
[42] He, M.X., Liu, Z.S., Du, K.P., Li, L.P., Chen, R., Carder, K.L., and Lee, Z.P., "Retrieval of chlorophyll from remote-sensing reflectance in the China seas," Applied Optics 39(15), 2467–2474 (2000).